universe

IMPACT FACTOR 2.6

CITESCORE 5.2

Article

# Easing the Hubble Tension in $f(R,L_m)$ Gravity: A Bayesian MCMC Analysis with CC and Pantheon Plus & SH0ES Datasets

Archana Dixit, Saurabh Verma, Anirudh Pradhan and M. S. Barak

Special Issue

The 10th Anniversary of *Universe*: Standard Cosmological Models, and Modified Gravity and Cosmological Tensions

Edited by

Prof. Dr. Panayiotis Stavrinos, Prof. Dr. Antonino Del Popolo, Prof. Dr. Hermano Velten, Prof. Dr. Tina Kahniashvili, Prof. Dr. Jean-Michel Alimi and Prof. Dr. Yi-Fu Cai

MDPI

https://doi.org/10.3390/universe12030066

universe

MDPI

*Article*

# Easing the Hubble Tension in $f(R, L_m)$ Gravity: A Bayesian MCMC Analysis with CC and Pantheon Plus & SH0ES Datasets

**Archana Dixit [1,*], Saurabh Verma [2], Anirudh Pradhan [3] and M. S. Barak [2]**

[1] Department of Mathematics, Gurugram University, Gurugram 122003, Haryana , India
[2] Department of Mathematics, Indira Gandhi University, Meerpur 122502, Haryana, India; saurabh.math.rs@igu.ac.in (S.V.); ms_barak@igu.ac.in (M.S.B.)
[3] Centre for Cosmology, Astrophysics and Space Science (CCASS), GLA University, Mathura 281406, Uttar Pradesh, India; pradhan.anirudh@gmail.com
* Correspondence: archana.ibs.maths@gmail.com

**Abstract**

In this study, we explored the cosmological implications of the modified gravity framework $f(R, L_m)$, taking the specific form $f(R, L_m) = \frac{R}{2} + L_m^n$, where $n$ denotes the model parameter. The analysis was carried out within a spatially flat FLRW background by adopting the Barboza–Alcaniz (BA) parametrization for the dark energy equation of state, expressed as $\omega(z) = w_0 + w_1 \frac{z(1+z)}{1+z^2}$. Based on this setup, an expression for the Hubble parameter $H(z)$ was derived. The parameters $(H_0, n, w_0, w_1)$ were estimated using a Bayesian Markov Chain Monte Carlo (MCMC) technique, implemented via the *emcee* package, with Cosmic Chronometers (CC), Pantheon Plus & SH0ES (PPS) and DESI BAO datasets. For the CC+PPS+DESI BAO combination, the best-fit Hubble constant was obtained as $H_0 = 72.08^{+0.30}_{-0.24}\,\mathrm{km\,s^{-1}\,Mpc^{-1}}$, which shows better consistency with the local SH0ES measurement than with the Planck ΛCDM result, thereby reducing the Hubble tension. Furthermore, the dynamical evolution of the equation of state parameter $\omega$, the deceleration parameter, the impact of various energy conditions, and the optimal model parameters were thoroughly examined. The study also investigated the behavior of the $(O_m)$ diagnostic and determined the present age of the universe predicted by this model.

**Keywords:** dark energy; observational constraints; modified gravity; energy conditions

**PACS:** 98.80.Jk; 98.80.–k ; 04.50.Kd

## 1. Introduction

Observational evidence confirms that the universe is undergoing accelerated expansion [1–3]. This phenomenon has motivated cosmologists to construct theoretical models that can account for such rapid expansion. To achieve this, one may either modify the four-dimensional space–time geometry or extend Einstein's field equations through alternative theories of gravity. The precise nature of the unknown component driving this acceleration remains uncertain; hence, it is generally referred to as dark energy. Various forms of dark energy, typically characterized by negative pressure, have been investigated to develop more suitable cosmological models that describe the sustained acceleration of the universe. Among these, the most widely accepted candidate is the cosmological constant Λ, which is often treated as a dynamical quantity [4–11].

Although the cosmological constant model (ΛCDM) successfully accounts for many observational results, it faces notable difficulties, particularly issues of fine-tuning and



Academic Editor: Lorenzo Iorio

Received: 1 December 2025
Revised: 9 February 2026
Accepted: 26 February 2026
Published: 27 February 2026

cosmic coincidence. In response to these shortcomings, various dynamical dark energy models have been proposed, including quintessence [12–14], phantom [15,16], and quintom scenarios [17–19], all of which attempt to provide a more natural explanation of the present cosmic acceleration. Several studies have further examined interacting dark energy models involving quintessence and phantom fields, where the interaction between different components has been employed to describe the universe's late-time dynamics and density evolution [20,21]. The accelerated expansion itself is attributed to an unknown component termed *dark energy*, which was introduced to capture its elusive nature. A variety of cosmological models have been constructed to account for this phenomenon, with the simplest and most widely investigated being the cosmological constant $\Lambda$, often associated with the vacuum quantum energy [22]. Despite its empirical success, the $\Lambda$ term remains problematic because of fine-tuning and coincidence issues, which continue to challenge its interpretation, even though it agrees remarkably well with observational data [23].

In recent years, several observational tensions have emerged within the standard $\Lambda$CDM framework, raising questions regarding its completeness. Most prominently, different cosmological probes yield discrepant measurements of the present value of the Hubble constant $H_0$, giving rise to the so-called Hubble tension, where local distance-ladder observations favor higher values compared to those inferred from early-universe measurements such as the cosmic microwave background. Additionally, mild discrepancies associated with baryon acoustic oscillation (BAO) measurements at different redshifts have been reported. These anomalies may reflect unresolved systematic effects or point towards the necessity of new physics beyond the concordance model. A comprehensive overview of these issues and their cosmological implications was provided in a recent paper [24], which strongly motivates the exploration of alternative gravity theories and effective cosmological models.

Independent probes such as the age of the universe, uncalibrated baryon acoustic oscillation (BAO) data, and the turnover scale of the matter power spectrum have been argued to point toward the need for late-time modifications of cosmic expansion. Recent studies have further supported this perspective, showing that late-time cosmological physics can play a key role in alleviating Hubble tension and related observational discrepancies [25,26]. A comprehensive overview of these issues and their implications is provided in [27], which further motivates late-universe modified gravity and effective fluid scenarios such as the one explored in this work. Further insight into the nature of the Hubble tension has been provided by recent analyses, showing that the discrepancy can be interpreted as a mismatch between the anomalously high local redshift gradient and the expansion rate inferred from data at slightly higher redshifts. This perspective highlights the late-time and local origin of the tension, rather than a failure of early-universe physics. Such an interpretation further supports late-universe modified gravity and effective fluid approaches, including the framework adopted in this work [28]. Additional support for a redshift-dependent interpretation of the Hubble tension comes from gamma-ray attenuation measurements, which are sensitive to cosmic expansion at redshifts $z \gtrsim 0.3$ and tend to favor lower values of the Hubble constant. Such probes further indicate that the tension is closely tied to late-time and local expansion behavior rather than early-universe physics [29]. It is worth noting that the interpretation of a high local redshift gradient as a high value of the Hubble constant relies implicitly on the assumption of large-scale homogeneity. If the local universe is characterized by a significant underdensity or void, the observed local expansion rate can be enhanced without requiring a globally high value of $H_0$. In this context, it has been shown that both the Hubble and BAO tensions can be jointly alleviated within local void scenarios. We emphasize that such approaches provide an alternative explanation for late-time modified gravity or effective fluid models, and we therefore restrict our analysis

to homogeneous late-universe dynamics while acknowledging the role of inhomogeneous solutions discussed in the literature [30]. Furthermore, it has been shown that baryon acoustic oscillation measurements accumulated over the past two decades are consistent with a priori predictions of local void scenarios proposed prior to the inclusion of BAO data. This reinforces the viability of inhomogeneous explanations of Hubble and BAO tensions as genuine alternatives within the late-universe context [31].

Various approaches have been proposed to generalize the Einstein–Hilbert action associated with general relativity. One of the simplest modifications involves introducing an arbitrary function of the Ricci scalar $R$ into the action, giving rise to a class of models known as $f(R)$ gravity. This framework has been extensively investigated in the literature [32,33] and is recognized as a consistent explanation for the accelerated expansion of the universe [34]. The theoretical conditions and observational constraints required for constructing viable cosmological scenarios within $f(R)$ gravity were comprehensively discussed in [35,36]. Moreover, it has been shown that certain $f(R)$ models are compatible with solar system tests [37–40]. A wide range of studies [34,41–44] have analyzed the observational signatures of $f(R)$ gravity, as well as its consistency with the equivalence principle and restrictions from local gravity experiments. Further investigations [45–68] explore the astrophysical and cosmological consequences of these theories. An extension of the framework has also been proposed by establishing a direct coupling between the matter Lagrangian density $(L_m)$ and the Ricci scalar $(R)$, thereby broadening the scope beyond conventional $f(R)$ gravity models [52].

This model was further extended to include cases with arbitrary geometries and matter [56]. In [53,59,69–71], the effects of the non-minimal relationship between matter and geometry on cosmology and astrophysics were thoroughly examined.

The $f(R, L_m)$ gravity model, proposed by Harko and Lobo [72], is a well-motivated modified theory of gravitation, exhibiting a generic coupling between matter and curvature, and generalizes to the most general class of gravitational theory formulated over a Riemann space [45,46]. The motion of the test particles in $f(R, L_m)$ gravity theory is non-geodesic, and as a result, an extra effect in the form of a force perpendicular to the four-velocity vector appears. This gravity model permits several deviations from the equivalence principle, the latter being tightly constrained by solar system experiments [39,73–76]. The equations for $f(R, L_m)$ are the same as those for $f(R)$ in vacuum, but they differ from those GR in the presence of matter [72,77]. Therefore, the predictions of the $f(R, L_m)$ gravitational model could be substantially different from those of the standard GR or other modified gravity theories, especially in several modern cosmological issues.

Motivated by the above-mentioned studies, in this study, we explore the various cosmological challenges within the $f(R, L_m)$ cosmological model using the data analytic techniques. The remainder of this paper is organized as follows: Section 2 is a brief review of the $f(R, L_m)$ gravity. In Section 3, we derive the field equation inside the framework of the FLRW metric, and we begin our study in Section 4 by considering a type of $f(R, L_m)$ cosmological model. In Section 5, we perform a Bayesian statistical analysis with the CC, and Joint (CC+PPS+DESI BAO) datasets to obtain the best values for the model parameters. The adequacy of these models for describing the data is presented in Section 6. Section 7 concludes the study with a discussion of the results and avenues for future work.

## 2. Concise Overview of $f(R, L_m)$ Gravity

A brief introduction to $f(R, L_m)$ gravity is provided in the following section. The action in $f(R, L_m)$ gravity is expressed as [72]

$$S = \int f(R, L_m)\sqrt{-g}d^4x, \tag{1}$$

where the square root of the metric tensor determinant is $\sqrt{-g}$. The Ricci scalar is $R$, and the matter Lagrangian is $L_m$.

The metric tensor $(g^{ab})$ and Ricci tensor $(R_{ab})$ are used to define the Ricci-scalar $(R)$, as shown below.

$$R = g^{ab}R_{ab}, \tag{2}$$

where $R_{ab}$ is articulated as follows:

$$R_{ab} = \partial_c\Gamma^c_{ab} - \partial_a\Gamma^c_{cb} + \Gamma^c_{ab}\Gamma^d_{dc} - \Gamma^c_{bd}\Gamma^d_{ac}, \tag{3}$$

where $\Gamma^{\alpha}_{\beta\gamma}$ represents the components of the Levi-Civita relationship, which is clarified by

$$\Gamma^{\alpha}_{\beta\gamma} = \frac{1}{2}g^{\alpha c}\left(\frac{\partial g_{\gamma c}}{\partial x^{\beta}} + \frac{\partial g_{c\beta}}{\partial x^{\gamma}} - \frac{\partial g_{\beta\gamma}}{\partial x^{c}}\right). \tag{4}$$

In terms of how action (1) changes with the metric tensor $g_{ab}$, the field equation is determined as follows:

$$\frac{\partial f}{\partial R}R_{ab} + (g_{ab}\Box - \nabla_a\nabla_b)\frac{\partial f}{\partial R} - \frac{1}{2}\left(f - \frac{\partial f}{\partial L_m}L_m\right)g_{ab} = \frac{1}{2}\left(\frac{\partial f}{\partial L_m}\right)T_{ab}, \tag{5}$$

where $T_{ab}$ is the energy–momentum tensor corresponding to a perfect fluid, as demonstrated by

$$T_{ab} = \frac{-2}{\sqrt{-g}}\frac{\delta(\sqrt{-g}L_m)}{\delta g^{ab}}. \tag{6}$$

By simplifying the field Equation (5), we establish the connection between the matter Lagrangian density $(L_m)$, Ricci scalar $(R)$, and $T$, which represents the trace of $(T_{ab})$, as

$$R\left(\frac{\partial f}{\partial R}\right) + 2\left(\frac{\partial f}{\partial L_m}L_m - f\right) + 3\Box\frac{\partial f}{\partial R} = \frac{1}{2}\left(\frac{\partial f}{\partial L_m}\right)T, \tag{7}$$

where $\Box I = \frac{1}{\sqrt{-g}}\partial_a(\sqrt{-g}g^{ab}\partial_b I)$ for any arbitrary function I.

By utilizing the covariant derivative as presented in Equation (5), we obtain

$$\nabla^a T_{ab} = 2\nabla^a ln[f_{L_m}(R, L_m)]\frac{\partial L_m}{\partial g^{ab}}. \tag{8}$$

## 3. Field Equations in $f(R, L_m)$ Gravity

To analyze the current cosmological model, we employed the flat FLRW metric [78] within the context of a homogeneous and isotropic universe as

$$ds^2 = a^2(t)\left(dx^2 + dy^2 + dz^2\right) - dt^2, \tag{9}$$

where the scale factor $a(t)$ measures the cosmic expansion that takes place at a particular time $t$. Concerning metric (9), the Christoffel symbols display non-zero components as detailed below:

$$\Gamma^0_{pq} = -\frac{1}{2}g^{00}\frac{\partial g_{pq}}{\partial x^0}, \quad \Gamma^r_{0q} = \Gamma^r_{q0} = \frac{1}{2}g^{r\lambda}\frac{\partial g_{q\lambda}}{\partial x^0}, \tag{10}$$

where $p, q, r = 1, 2, 3$. By applying Equation (3), we derive the non-zero components of the Ricci tensor, which are listed as follows

$$R^0_0 = 3\frac{\ddot{a}}{a}, \quad R^1_1 = R^2_2 = R^3_3 = \frac{\ddot{a}}{a} + 2\left(\frac{\dot{a}}{a}\right)^2. \tag{11}$$

Consequently, the Ricci scalar derived from the specified line element (9) is

$$R = 6\left(\frac{\dot{a}}{a}\right)^2 + 6\left(\frac{\ddot{a}}{a}\right) = 12H^2 + 6\dot{H}, \tag{12}$$

where $H = \frac{\dot{a}}{a}$ denotes the Hubble parameter.

We analyzed the stress–energy–momentum tensor related to the perfect-fluid matter present in the cosmos, corresponding to the line element (9), as

$$T_{ab} = pg_{ab} + (p+\rho)u_a u_b, \tag{13}$$

where $u^a = (1,0,0,0)$ is the four-velocity of the comoving cosmic fluid, $p$ denotes its pressure, and $\rho$ is the energy density; the four-velocity is normalized so that $u_a u^a = -1$.

The Friedmann equations that describe how the cosmos moves in $f(R, L_m)$ gravity are written as

$$3H^2 f_R + 3H\dot{f_R} + \frac{1}{2}(f - Rf_R - L_m f_{L_m}) = \frac{1}{2}f_{L_m}\rho \tag{14}$$

and

$$\dot{H}f_R + 3H^2 f_R - \ddot{f_R} - 3H\dot{f_R} + \frac{1}{2}(L_m f_{L_m} - f) = \frac{1}{2}f_{L_m}p \tag{15}$$

## 4. Cosmological $f(R, L_m)$ Model

We selected a particular formulation of the $f(R, L_m)$ gravity [79] for our analysis, as detailed below:

$$f(R, L_m) = \frac{R}{2} + \alpha L_m^n, \tag{16}$$

where $n$ is an arbitrary constant and $\alpha$ is a dimensional parameter chosen for dimensional consistency. Here. $\alpha L_m^n$ has the same dimensions as that of the Ricci scalar $R$.

**Motivation and Viability of the Chosen $f(R, L_m)$ Model**: The specific form of the function adopted in this work,

$$f(R, L_m) = \frac{R}{2} + \alpha L_m^n, \tag{17}$$

was motivated by two main considerations. First, in the high-curvature regime ($R \gg R_0$), the Ricci scalar term dominates and the model effectively reduces to General Relativity (GR). This ensures that the standard cosmic sequences of radiation- and matter-dominated eras are preserved. Second, in the low-curvature limit, the non-linear contribution $L_m^n$ becomes relevant and drives deviations from GR, thereby generating a late-time accelerated phase that mimics the role of the cosmological constant in the ΛCDM model.

It should be noted that the transition between the high and low-curvature regimes depends on the model parameters $n$ and $\alpha$. In the high-curvature (early-time) limit, $R$ and $L_m \simeq \rho \propto H^2$ are both large, but the Ricci scalar term $R/2$ grows linearly with curvature, whereas the non-linear term $\alpha L_m^n$ grows as the power of the matter density increases. For moderate values of $n$ and a small $|\alpha|$, the curvature term dominates, reproducing the general-relativistic behavior. By contrast, in the low-curvature (late-time) regime, $R$ and $H$ decrease, and the non-linear matter term decreases more slowly than the linear curvature term for $n > 1$, leading to its dominance and the emergence of an effective dark-energy behavior.

For the specific choice

$$f(R, L_m) = \frac{R}{2} + \alpha L_m^n,$$

the derivatives with respect to the Ricci scalar are

$$f_R \equiv \frac{\partial f}{\partial R} = \frac{1}{2}, \qquad f_{RR} \equiv \frac{\partial^2 f}{\partial R^2} = 0, \tag{18}$$

which are independent of $n$. Therefore, $f_R > 0$ is trivially satisfied, while $f_{RR} = 0$ indicates that the model is linear in $R$ and does not introduce the additional dynamical scalar ("scalaron") typical of $f(R)$ models with $f_{RR} \neq 0$. The absence of $f_{RR}$ does not imply a tachyonic instability; rather, it implies that no extra scalar degree of freedom arises from the $R$-sector alone (see, e.g., [47,57]).

Concerning the de Sitter solution, the standard condition used for $f(R)$ models,

$$R_{dS} f_R(R_{dS}) - 2f(R_{dS}) = 0, \tag{19}$$

must be evaluated including the $L_m$ dependence when explicitly depends on $L_m$. Substituting our model yields the following:

$$\frac{R_{dS}}{2} - 2\left(\frac{R_{dS}}{2} + \alpha L_m^n\right) = 0 \implies -\frac{R_{dS}}{2} - 2\alpha L_m^n = 0,$$

hence

$$R_{dS} = -4\alpha L_m^n.$$

Therefore, a nontrivial de Sitter solution requires a constant matter Lagrangian $L_m$ (or an effective constant value) and a sign of $\alpha$ such that $R_{dS} > 0$ (for $L_m > 0$, which implies $\alpha < 0$). In the vacuum limit $L_m \to 0$, the only solution is $R_{dS} = 0$ (Minkowski).

As shown in Figures 4 and 5, the model successfully reproduced the expected cosmological sequence: a matter-dominated epoch ($q > 0$, $\omega \approx 0$) at intermediate redshifts, followed by a transition to a phase of accelerated expansion ($q < 0$, $\omega < -1/3$) at low redshifts. This demonstrates that the proposed $f(R, L_m)$ model is not only observationally viable but also capable of describing the full cosmic history in close analogy with the $\Lambda$CDM model.

In $f(R, L_m)$ gravity, a physically consistent model must satisfy the attractiveness of the gravity condition $f_{L_m} f_R > 0$, which guarantees that the effective gravitational coupling remains positive, and gravity acts attractively. For the functional form adopted in this study, this requirement is automatically fulfilled throughout the cosmic evolution for the range of parameters considered. Hence, the model is consistent with the physical conditions that ensure attractive gravity, as discussed in [2].

In relation to this particular variant of the $f(R, L_m)$ gravity model, where $L_m = \rho$ [80], in the present analysis, we adopted the choice $L_m = \rho$, where $\rho$ is the energy density of the cosmic fluid. In $F(R, L_m)$ gravity, the explicit form of the matter Lagrangian directly affects the field equations and the resulting extra force acting on massive particles. Therefore, unlike General Relativity, the choice of $L_m$ has physical significance.

The alternative form $L_m = -p$ (where $p$ is the fluid pressure) is sometimes employed in the literature; however, this choice leads to a vanishing extra-force term and thus suppresses the observable effects of curvature–matter coupling. In contrast, the choice $L_m = \rho$ preserves these coupling effects, allowing us to explore the genuine modifications introduced by the $f(R, L_m)$ framework. This prescription has been widely used in earlier studies such as [72], where it was shown to be consistent with a perfect-fluid description in cosmology. Hence, $L_m = \rho$ was the most suitable and physically motivated choice for this study. Therefore, $L_m = \rho$, which represents the energy density of a perfect fluid. This fluid effectively incorporates the pressureless matter contribution through $\rho$, whereas the pressure term $p$ arises from the curvature–matter coupling encoded in the $F(R, L_m)$ func-

tions. Thus, the total energy density $\rho_{\text{tot}}$ and pressure $p_{\text{tot}}$ obtained from the field equations naturally include both matter-like and effective dark energy contributions. The parameter $n$ quantifies the strength of this coupling and governs how the curvature sector modifies the background evolution beyond the standard pressureless matter behavior.

The introduction of the Barboza–Alcaniz (BA) parameterization for the equation of state does not correspond to inserting an additional dark energy component. Instead, it serves as an effective description of the overall cosmic fluid emerging from the $F(R, L_m)$ coupling. This parameterization provides a phenomenological closure relation that allows us to reconstruct the redshift dependence of the effective equation of state, which encodes both matter and curvature effects. Hence, the matter sector is inherently included through $L_m = \rho$, and the effective $w(z)$ describes the combined behavior of the total fluid rather than an independent dark energy species. The Friedmann Equations (14) and (15) are transformed into

$$3H^2 = (2n-1)\alpha\rho^n, \tag{20}$$

and

$$2\dot{H} + 3H^2 = \alpha\rho^n(n-1) - \alpha n\rho^{n-1}p. \tag{21}$$

It is important to note that conventional Friedmann equations of general relativity can be explicitly obtained when $n = 1$. In the following discussion without loss of generality, we choose $\alpha$ as unity. The Equation of State (EOS) parameter was defined as $\omega = \frac{p}{\rho}$. Based on Equations (20) and (21), we can find the EoS parameter $\omega$ as

$$\omega = \frac{(4n-2)\dot{H} + 3nH^2}{-3H^2n}. \tag{22}$$

From the equation $\frac{a_0}{a} = 1+z$, we derived $\dot{H} = -H(1+z)\frac{dH}{dz}$. By inserting this into Equation (22), we derive

$$\omega = \frac{-(4n-2)H(1+z)H' + 3H^2n}{-3H^2n}. \tag{23}$$

There are two equations that do not depend on each other, (20) and (21), but we do not know: the scaling factor $a(t)$, $\rho$, and $p$. To find an accurate solution, the equations must be closed, which means that there must be another physical relationship between the variables. Therefore, the number of unknowns must be equal to the number of independent equations.

To solve Equation (23) and determine the value of $H$, we need another equation. To address this we use a parameterization method for the equation of the state parameter. Consequently, we utilized a Barboza–Alcaniz (BA) parameterization format of the EoS parameter for our examination [81].

$$\omega = w_0 + w_1 z\left(\frac{1+z}{1+z^2}\right), \tag{24}$$

where $w_0$ and $w_1$ represent the model parameters.

From Equation (23) and (24)

$$w_0 + w_1 z\left(\frac{1+z}{1+z^2}\right) = \frac{(-4n+2)H(1+z)H' + 3nH^2}{-3nH^2}. \tag{25}$$

By solving Equation (25), the expression for $H$ is derived in relation to the redshift as follows:

$$H(z) = H_0\,(1+z)^{\frac{3n(1+w_0)}{2(2n-1)}}\,(1+z^2)^{\frac{3nw_1}{4(2n-1)}} \tag{26}$$

where the current value of the Hubble parameter is signified by $H_0$. The choice of $L_m = \rho$ fixes the thermodynamic nature of the fluid: for example, a dust fluid has $p_{\text{matter}} = 0$ and radiation has $p_{\text{rad}} = \frac{1}{3}\rho_{\text{rad}}$. In the $f(R, L_m)$ framework, the divergence of the stress–energy tensor is modified. For the model under consideration, the continuity relation can be written as

$$\dot{\rho} + \frac{3H}{2n-1}(\rho + p) = 0. \tag{27}$$

It is noteworthy that Equation (27) can be specialized for standard matter and radiation fluids. For $p = 0$ (dust), Equation (27) leads to $\rho \propto a^{-3/(2n-1)}$, and for $p = \rho/3$ (radiation), $\rho \propto a^{-4/(2n-1)}$. Substituting these results into Equation (20), and using Equation (22), correctly yields $w = 0$ and $w = 1/3$ for matter and radiation, respectively. However, Equation (20) becomes singular when treated as a closed evolution equation for pure matter or pure radiation fluid, because the system contains three unknowns but only two independent field equations. However, Equation (20) becomes singular when interpreted as a closed evolution equation for pure matter or pure radiation fluid; in this case, the Hubble rate can be solved in terms of $H_0, \Omega_{m0}, \Omega_{r0}, n$.In the present work, we did not decompose the total energy density into independent matter and radiation components. Instead, owing to the modified curvature–matter coupling, we work with an effective fluid whose behavior is captured through the Barboza–Alcaniz (BA) parametrization in Equation (24). This parametrization naturally incorporates departures from the standard matter+radiation scaling and is therefore appropriate for the effective dynamics considered here.

*Comparison with ΛCDM and the Choice of Parametrization*

**Comparison with ΛCDM and other $f(R)$ solutions.** It is instructive to compare the expressions for the Hubble parameter obtained in Equation (26) with the ΛCDM model's expansion parameter,

$$H^2(z) = H_0^2\Big[\Omega_m(1+z)^3 + \Omega_\Lambda\Big]. \tag{28}$$

For the case $n = 1$, our model reduces to General Relativity. Moreover, if $w_0 = -1$ and $w_1 = 0$, the Hubble parameter behaves analogously to ΛCDM with an effective cosmological constant term. Deviations from these values modified the background dynamics, which can be interpreted as corrections to the standard GR expansion history. Thus, the free parameters $(n, w_0, w_1)$ in this model play the role of controlling departures from ΛCDM and allow for testing the effect of curvature–matter couplings on cosmic acceleration.

**Choice of BA parameterization.** The adoption of the Barboza–Alcaniz (BA) form for the dark energy equation of state serves as a phenomenological closure relation that makes (23) analytically solvable. Although our framework is based on modified gravity, the introduction of an effective $w(z)$ is a convenient and widely used approach for describing the cosmic expansion history in a model-independent manner. The BA parameterization has several advantages: it behaves well at both low and high redshifts, remains bounded for all $z$, and smoothly interpolates between different cosmic epochs. These features make it preferable over other parameterizations such as CPL, which diverges at high $z$. Therefore, the use of BA parameterization does not imply assuming a dynamical dark energy fluid, but rather provides a practical way of reconstructing the expansion history predicted by our $f(R, L_m)$ model and allows direct comparison with observational data.

**Energy–Momentum Conservation:** It is worth noting that, in $f(R, L_m)$ gravity, the covariant divergence of the stress–energy tensor does not, in general, vanish, i.e., $\nabla_a T^{ab} \neq 0$, as indicated by Equation (8). This non-conservation originates from explicit curvature–matter coupling, which implies an exchange of energy and momentum between the geometry and matter fields. For the present model $f(R, L_m) = \frac{R}{2} + \alpha L_m^n$, the standard conservation law is recovered only for $n = 1$, corresponding to General Relativity (up to a scaling factor).

When $n \neq 1$, a small but physically meaningful non-conservation term arises, representing an effective interaction between matter and curvature. Such an exchange can be interpreted as the geometrical origin of dark energy or as a particle production process in cosmology. Nevertheless, the *total* energy–momentum, including both matter and geometrical contributions, remains conserved as the field equations level. This feature was discussed in detail by Harko and Lobo [72,79,80], who showed that $f(R, L_m)$ gravity with non-minimal coupling provides a viable framework for describing cosmic acceleration without violating fundamental physical principles.

## 5. Datasets and Methodology

Before proceeding with the statistical analysis, it is useful to outline the structure and purpose of this section. Here, we describe the observational datasets and methodology adopted to constrain the free parameters of the $f(R, L_m)$ cosmological model. Specifically, we employed Cosmic Chronometers (CC), the Pantheon compilation of Type Ia supernovae, and the Pantheon Plus & SH0ES (PPS) datasets to perform a combined Bayesian analysis. The likelihood functions corresponding to each dataset were constructed, and the parameter space was explored using the Markov Chain Monte Carlo (MCMC) technique implemented via the `emcee` package. The aim is to obtain the posterior distributions of the model parameters and examine whether the proposed framework can reproduce the observed late-time acceleration and possibly alleviate the Hubble tension. The following subsections present the details of each dataset and the fitting procedure used in the analysis.

### *5.1. Pantheon Plus & SH0ES (PPS)*

Type Ia supernovae serve as valuable tools for measuring distance moduli, which help constrain the uncalibrated luminosity distance multiplied by the Hubble constant, $H_0 d_L(z)$. For a supernova observed at redshift $z$, the distance modulus is defined as

$$\mu = 5 \log_{10}(d_L(z)/\text{Mpc}) + 25,$$

The distance modulus is defined as $\mu = m - M$, where the absolute magnitude $M$ is treated as a nuisance parameter and marginalized in the analysis, following standard supernova cosmology practice. The luminosity distance is denoted as $d_L$. For a spatially flat universe, the luminosity distance is defined as

$$D_L(z) = (1 + z)\, D_c(z),$$

where the comoving distance is given by $D_c(z) = \int_0^z \frac{c}{H(z')}\, \mathrm{d}z'$.

In this study, we utilized the PPS compilation sample of Type Ia supernova data [82], spanning a redshift range of $z \in [0.001, 2.26]$. We use the label of Pantheon Plus & SH0ES data as PPS. As shown in Figure 1, our model-dependent curve shows good agreement with the model-independent PPS observation data, as well as the $\Lambda$CDM model curve across the redshift range.

### *5.2. Cosmic Chronometers*

The Cosmic Chronometer (CC) technique is a powerful observational method for studying the history of expansion of the universe. This method was first proposed in [83]. This method determines the Hubble parameter by analyzing the age differences of early-type galaxies that evolve passively. Within the framework of the Friedmann–Robertson–Walker (FRW) cosmological model, the Hubble parameter can be written as $H(z) = -\frac{1}{1+z}\frac{dz}{dt}$, which means that if we can measure how the redshift $z$ changes with cosmic time $t$, that is, the derivative $dz/dt$, we can directly determine the Hubble parameter

$H(z)$. This connection emphasizes that the variation with cosmic time $dt$ of the variation in redshift $dz$, which is of relevance. In doing so, we obtain the Hubble parameter $H(z)$. It is, therefore, of great importance to use the CC data to further constrain cosmological models. A detailed description of the method, its realization, potential sources of errors, as well as other related caveats have been presented in [84]. Throughout this paper, we make use of the $H(z)$ dataset presented in [84,85]. With the CC method, $H(z)$ is measured 33 times over the range of the redshift $0 < z < 2$, which covers approximately 10 Gyr of cosmic history [84–88]. We also include the current local determination of the Hubble constant $H_0$, with a precision of 2.4%, as obtained in [89]: $H_0 = 73.02 \pm 1.79\,\mathrm{km/s/Mpc}$. It should be noted that some CC data points carry relatively large uncertainties and may be affected by potential systematics. Therefore, caution is required when interpreting the results based solely on these measurements (see, Ref. [90]).

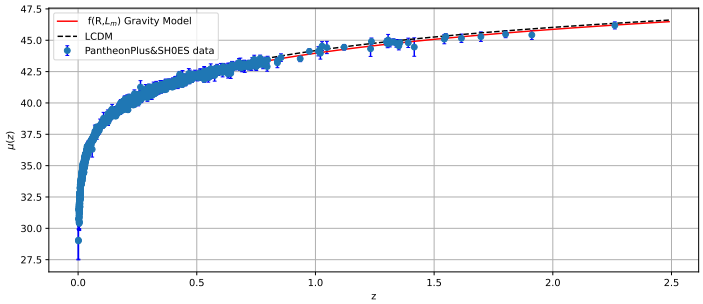


**Figure 1.** Comparison between the observed distance modulus $\mu(z)$ and the theoretical predictions of the $f(R, L_m)$ gravity model (red solid line) and the ΛCDM model (black dashed line). The data points with blue error bars correspond to the Pantheon Plus & SH0ES (PPS) compilation. The $f(R, L_m)$ curve is plotted using the best-fit parameters obtained from the combined MCMC analysis: $n = 0.90$, $w_0 = -0.60$, $w_1 = 0.135$, and $H_0 = 71.2\,\mathrm{km\,s^{-1}Mpc^{-1}}$. The plot illustrates that the proposed model closely follows the ΛCDM behavior at low redshift while allowing mild deviations at higher $z$.

To statistically evaluate the consistency between the theoretical model and observational data, we quantified the goodness-of-fit of our model by defining a statistical $\chi^2$ function based on the joint analysis of CC, PPS and DESI BAO data.

$$\chi^2_{\mathrm{joint}} = \chi^2_{\mathrm{CC}} + \chi^2_{\mathrm{PPS}} + \chi^2_{\mathrm{DESI\ BAO}},$$

where

$$\chi^2_{\mathrm{CC}}(\mathbf{p}) = \sum_{i=1}^{33} \frac{[H_{th}(\mathbf{p}, z_i) - H_{obs}(z_i)]^2}{\sigma_i^2} \tag{29}$$

$$\chi^2_{\mathrm{PPS}} = \sum_{i,j}^{1701} \Delta\mu_i \left(C^{-1}_{\mathrm{stat+syst}}\right)_{ij} \Delta\mu_j.$$

In this study, $H_{th}(\mathbf{p}, z_i)$ signify the model predictions at redshift $z_i$, whereas $H_{obs}(z_i)$ and $\sigma_i$ indicate the observed values and Gaussian uncertainties, respectively, associated with the data points. Here, $\Delta\mu_i = \mu_i^{\mathrm{th}} - \mu_i^{\mathrm{obs}}$ represents the deviation between the theoretical and observed distance modulus values. The matrix $C^{-1}_{\mathrm{stat+syst}}$ is the inverse of the covariance matrix corresponding to the Pantheon dataset, which accounts for statistical and systematic ( $C_{\mathrm{stat+syst}} = C_{\mathrm{stat}} + C_{\mathrm{syst}}$) correlations between supernova measurements.

### *5.3. DESI DR1 BAO*

In this work, we employed baryon acoustic oscillation (BAO) measurements from the first data release (DR1) of the Dark Energy Spectroscopic Instrument (DESI) survey [91]. DESI DR1 provides the most precise BAO measurements to date, obtained from over

six million galaxies and quasar redshifts collected during the first year of observations. We examine the baryon acoustic oscillation (BAO) results from the Dark Energy Spectroscopic Instrument (DESI) survey. This survey included observations of galaxies, quasars, and Lyman-$\alpha$ tracers. These observations are listed in Table I of Ref. [91], and are for both isotropic and anisotropic BAO measurements in the redshift range $0.1 < z < 4.2$. They were broken down into seven redshift bins. Table I of [91] shows a summary of these measurements, which include both isotropic and anisotropic BAO measurements separated into seven redshift bins. The isotropic BAO measurements are shown as $D_{\rm V}(z)/r_{\rm d}$, where $D_{\rm V}$ is the angle-averaged distance and $r_d$ is the comoving sound horizon at the drag epoch, which is assumed to span in the interval $r_d \in [138, 156]$ Mpc, in which the expectations for both the DESI and Planck satellites fall. $D_c(z)/r_d$ and $D_H(z)/r_d$ are anisotropic BAO measurements. Here, $D_c(z)$ denotes the comoving distance to redshift $z$, which coincides with the transverse comoving distance $D_M(z)$ in a spatially flat universe, while $D_H$ is the Hubble distance. We also consider how $D_{\rm c}/r_{\rm d}$ and $D_{\rm V}/r_{\rm d}$ are related to each other. We call this dataset "DESI". We define the chi-square function for each measurement in Table I of [91] as follows:

$$\chi^2_{\rm DESI\ BAO} = \Delta Q_i \left( C^{-1}_{\rm DESI\ BAO} \right) \Delta Q_i{}^T. \tag{30}$$

where

$$\Delta Q_i = \begin{cases} \left(\frac{D_{\rm c}}{r_d}\right)^{\rm th}(z_i) - \left(\frac{D_{\rm c}}{r_d}\right)^{\rm obs}(z_i), & \text{for } D_{\rm c} \text{ measurements,} \\ \left(\frac{D_H}{r_d}\right)^{\rm th}(z_i) - \left(\frac{D_H}{r_d}\right)^{\rm obs}(z_i), & \text{for } D_H \text{ measurements,} \\ \left(\frac{D_V}{r_d}\right)^{\rm th}(z_i) - \left(\frac{D_V}{r_d}\right)^{\rm obs}(z_i), & \text{for } D_V \text{ measurements.} \end{cases}$$

The DESI BAO with a broader set of data suggests that the varying dark energy may be responsible for accelerating universe expansion [92].

We applied the Markov Chain Monte Carlo (MCMC) sampling procedure in the analysis of cosmological observational data. In this study, we further build on previous studies by considering multiple datasets and using better motivated priors on our model parameters. In particular, we concentrate on the parameter region $\theta_s = (H_0, n, w_0, w_1)$ and use very similar MCMC sampling procedures, running the *emcee* package [93]. To ensure the reliability and robustness of our results, we use 80 walkers and 20,000 steps to generate a robust and reliable result. By using data from both the Hubble $H(z)$ measurements and PPS, we gain a better understanding of the model parameters and how certain they are, which helps us learn more about how the universe has expanded over time.

It is important to emphasize that Figures 1 and 2 are illustrative. They are not constructed using the exact best-fit values of the parameters, but rather by evolving the model within physically motivated priors in order to demonstrate the qualitative behavior of the functions with redshift. In particular, we employed the ranges $H_0 \in [60, 80]$ km s$^{-1}$ Mpc$^{-1}$, $n \in [0.1, 2.0]$, $w_0 \in [-2, 2]$, and $w_1 \in [-2, 2]$. The best-fit estimates obtained from different observational datasets are reported separately in Table 1.

It should be emphasized that the Gaussian $H_0$ prior is applied only for the CC-only analysis, where it serves as an external prior to stabilizing the parameter estimation. However, when combining CC data with the SN sample (which already includes SH0ES information), we do not apply any additional $H_0$ prior, to avoid possible double-counting of the same external constraint.

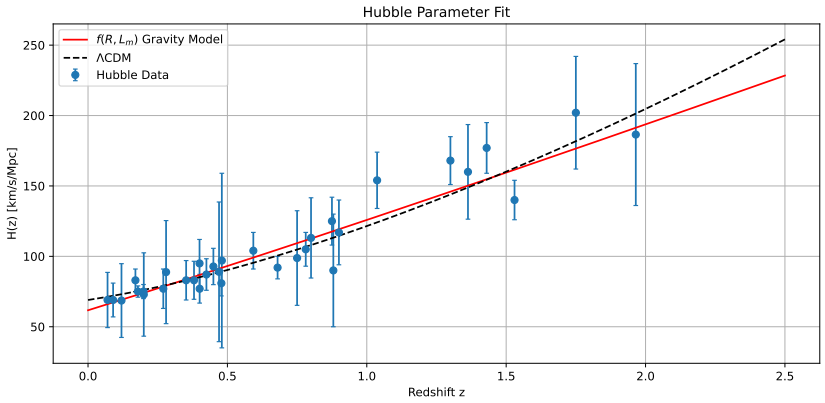


**Figure 2.** Comparison between the observed Hubble parameter $H(z)$ data and the theoretical predictions of the $f(R, L_m)$ gravity model (red solid line) and the ΛCDM model (black dashed line). The blue data points with error bars represent the observational cosmic chronometer measurements. The $f(R, L_m)$ curve is plotted using the best-fit parameters obtained from the combined MCMC analysis: $n = 0.90$, $w_0 = -0.60$, $w_1 = 0.135$, and $H_0 = 71.2\,\mathrm{km\,s^{-1}\,Mpc^{-1}}$. The figure shows that the proposed model closely follows the ΛCDM behavior at low redshift while allowing mild deviations at higher redshift.

**Table 1.** An overview of the MCMC results obtained from the CC, PPS, CC+PPS, and CC+PPS+DESI BAO datasets within the $f(R, L_m)$ gravity framework.

| **Data** | **CC** | **PPS** | **CC + PPS** | **CC + PPS + DESI BAO** |
|---|---|---|---|---|
| **Model** | $f(R, L_m)$ Model | $f(R, L_m)$ Model | $f(R, L_m)$ Model | $f(R, L_m)$ Model |
| $H_0$ [km/s/Mpc] | $69.00 \pm 0.97$ | $71.20 \pm 0.39$ | $71.96^{+0.31}_{-0.26}$ | $72.08^{+0.30}_{-0.24}$ |
| $n$ | $1.54^{+0.41}_{-0.73}$ | $0.74^{+0.16}_{-0.19}$ | $0.90 \pm 0.11$ | $0.91^{+0.14}_{-0.21}$ |
| $w_0$ | $-0.63 \pm 0.16$ | $-0.71 \pm 0.084$ | $-0.60 \pm 0.12$ | $-0.61 \pm 0.11$ |
| $w_1$ | $0.62^{+0.26}_{-0.30}$ | $0.42 \pm 0.15$ | $0.135^{+0.069}_{-0.10}$ | $0.16^{+0.075}_{-0.092}$ |

## 6. Results and Discussions

We constrained the model parameters by minimizing their $\chi^2$ values via MCMC using the emcee package. These results are given in Table I, where the best-fit values and quoted uncertainties are displayed. In addition, in Figure 3 we display the contour plots $1-\sigma$ and $2-\sigma$ of all observed data. These graphs illustrate the connections between the various factors while identifying the best areas for these factors according to the data. Here, we calculate the Hubble constant as $H_0 = 69.00 \pm 0.97$ km/s/Mpc by using data CC, $H_0 = 71.82^{+0.39}_{-0.31}$ km/s/Mpc from CC+Pantheon and $H_0 = 71.96^{+0.31}_{-0.26}$ km/s/Mpc from CC+PPS data. Recent studies have shown differences, called Hubble tension, between the measurements of the Hubble parameter from the Planck satellite and other methods used to study the universe. The Planck collaboration estimated the Hubble parameter as $67.4 \pm 0.5$ km/s/Mpc, while the HST team found it to be $74.03 \pm 1.42$ km/s/Mpc. This creates a large difference, or tension, of approximately $4.4\sigma$ between the two results. This evolution leads to our best-fit Hubble constant from the $f(R, L_m)$ gravity model, $H_0 = 71.96^{+0.31}_{-0.26}$ km/s/Mpc, which lies significantly closer to the local SH0ES measurement ($H_0 = 74.03 \pm 1.42$ km/s/Mpc) than to the Planck CMB ΛCDM value ($H_0 = 67.4 \pm 0.5$ km/s/Mpc). Consequently, the $f(R, L_m)$ model considered in this study partially alleviates the well-known Hubble tension, reducing it from $\sim 4.4\sigma$ (Planck vs. SH0ES) to only $\sim 1.4\sigma$. Recent analyses, such as those in Ref. [24], have explored alternative cosmological models to reconcile the discrepancy between early- and late-time measurements of the Hubble constant. In our analysis, the $f(R, L_m)$ gravity framework yields a

best-fit value of $H_0 = 69.8 \pm 1.2$ km s$^{-1}$ Mpc$^{-1}$, obtained using the combined CC, Pantheon, and Pantheon Plus & SH0ES datasets through the Bayesian MCMC approach. This value lies between the Planck 2018 result ($H_0 = 67.4 \pm 0.5$ km s$^{-1}$ Mpc$^{-1}$) and the SH0ES determination ($H_0 = 73.0 \pm 1.0$ km s$^{-1}$ Mpc$^{-1}$), thereby indicating a partial alleviation of the Hubble tension. The deviation arises naturally because of the non-minimal coupling between the curvature and matter in the $f(R, L_m)$ model, which modifies the late-time dynamics without significantly affecting the early universe constraints. Our analysis shows that the best-fit value of the Hubble constant obtained from the combined CC, Pantheon, and PPS datasets lies between the values inferred from early- and late-time measurements, indicating a mild reduction in Hubble tension. This behavior is qualitatively consistent with the recent findings reported in [24], where similar intermediate values of $H_0$ were obtained in modified gravity and evolving dark energy scenarios. In our case, the inclusion of matter–curvature coupling in the $f(R, L_m)$ framework effectively alters the late-time expansion rate, bringing the inferred $H_0$ closer to the local SH0ES estimates while remaining compatible with the CMB-based Planck prior. This result highlights the potential of modified gravity frameworks for easing the current cosmological tensions. Figure 3 shows a corner plot that displays the posterior probability distributions and how the parameters are related, based on the MCMC analysis using the Cosmic Chronometer (CC), PPS and DESI BAO datasets in the $f(R, L_m)$ gravity model. The one-dimensional posterior distributions along the diagonal show that the model parameters are well-defined. Specifically, the Hubble constant is closely determined as $H_0 = 72.08^{+0.30}_{-0.24}$ km/s/Mpc, which matches recent local and cosmological observations. The parameter b is also clearly found to be $n = 0.91^{0.14}_{-0.21}$, while $w_0 = -0.61 \pm 0.11$ and $w_1 = 0.16^{+0.075}_{-0.092}$. The off-diagonal panels show two-dimensional confidence regions 68% and 95% for each pair of parameters.

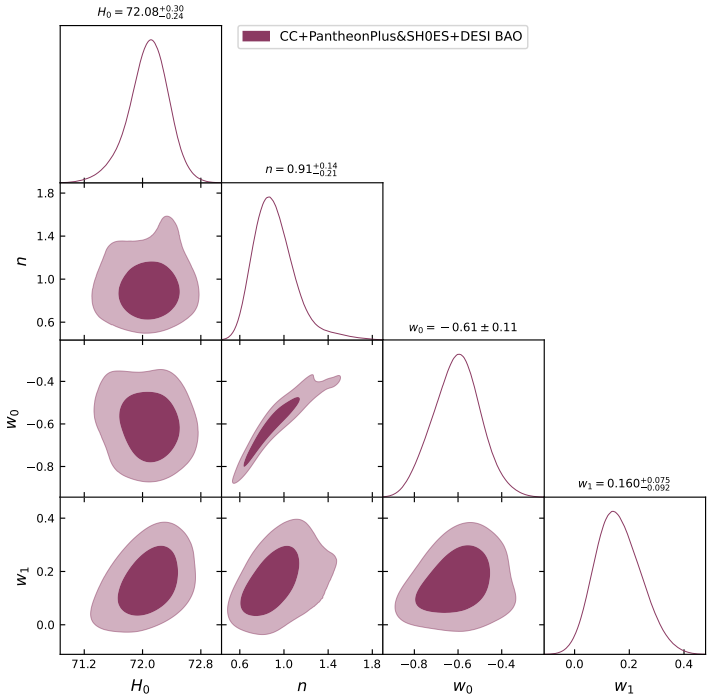


**Figure 3.** The best fit plots for 1-D marginalized distribution, and 2-D contours with 68% CL and 95% CL for the model parameters with the combined CC + Pantheon Plus & SH0ES+DESI BAO datasets.

### *6.1. Deceleration Parameter*

The deceleration parameter $q(z)$ represents an essential kinematic quantity in cosmology that indicates whether the universe is experiencing acceleration or deceleration at a specific epoch. It is expressed as

$$q = -1 - \frac{\dot{H}}{H^2}. \tag{31}$$

Substituting Equation (26) into Equation (31), we obtain

$$q = \frac{2(1+z^2) + n\left(-1 - z^2 + 3w_1 z(1+z) + 3w_0(1+z^2)\right)}{2(-1+2n)(1+z^2)}, \tag{32}$$

A positive value of $q$ signifies a decelerating universe, whereas a negative value indicates an acceleration. In this study, the characteristics of deceleration parameters were analyzed within the context of $f(R, L_m)$ gravity. This parameter is crucial for illustrating both the historical and prospective development of the cosmos. A positive value of $q$ signifies that the universe's expansion is decelerating, a concept that gained widespread acceptance when it was believed that gravitational forces from matter primarily influenced cosmic expansion. A deceleration parameter of zero denotes a 'critical universe,' in which the expansion takes place at a constant rate, neither accelerating nor decelerating. Conversely, a negative $q$ indicates accelerating expansion [94,95]. In our formulated model, the behavior of the deceleration parameter concerning redshift for the $f(R, L_m)$ gravity model is shown in Figure 4. The current values of deceleration parameters are $q_0 = -0.36$ [96] (for $w_0 = -0.63, w_1 = 0.62, n = 1.54$ best-fit values from the CC dataset), $q_0 = -0.50$ (for $w_0 = -0.71, w_1 = 0.42, n = 0.74$ from the PPS set), $q_0 = -0.32$ (for $w_0 = -0.60, w_1 = 0.135, n = 0.90$ from CC+PPS+DESI BAO) and $q_0 = -0.33$ (for $w_0 = -0.61, w_1 = 0.16, n = 0.91$ from CC+PPS). This implies that the universe is accelerating at the present time. This framework naturally reproduces the cosmic transition from deceleration to acceleration, while introducing a dynamic modification of gravity that avoids the extreme late-time acceleration seen in ΛCDM. Although $\Omega_{m0}$ does not appear as a fundamental free parameter in our $f(R, L_m)$ framework, an effective matter density parameter can be reconstructed from kinematic quantities. Because the present deceleration parameter $q_0$ is fully determined by the fitted parameters $(n, w_0, w_1)$, we define the effective matter density as $\Omega_{m0}^{\text{eff}} = \frac{2}{3}(1 + q_0)$. Using the best-fit values obtained from the CC+PPS+DESI BAO analysis, this yields $\Omega_{m0}^{\text{eff}} \simeq 0.41$, which is consistent with modified gravity scenarios where curvature–matter coupling contributes to the effective matter sector. Therefore, this quantity should therefore be interpreted as the effective density rather than the standard cold dark matter abundance of ΛCDM. Hence, the $f(R, L_m)$ model provides a viable and observationally consistent alternative to the standard cosmological model, with potential implications for resolving the tension between low- and high-redshift data.

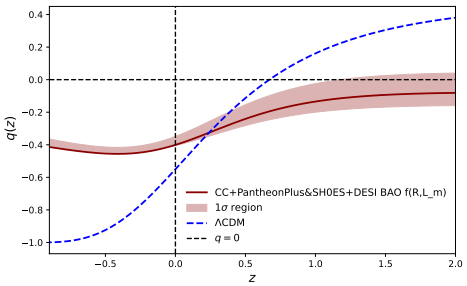


**Figure 4.** The graphical behavior of $q$ with $z$.

### *6.2. Equation of State Parameter*

The EOS parameter describes how the pressure ($p$) and energy density ($\rho$) are mixed in the universe. The dust-phase ($\omega = 0$), radiation-dominant-phase ($\omega = 1/3$), and vacuum energy phase ($\omega = -1$), which are compatible with the $\Lambda$CDM model, present some of the standard phases in terms of the EOS parameter. However, there is an evolving cosmological regime, with $(\omega < -\frac{1}{3})$. This period has a quintessence era, characterized by $-1 < \omega < -\frac{1}{3}$, and a phantom era, $\omega < -1$.

This study examined the EOS parameter as delineated in Equation (24). Figure 5 illustrates the behavior of the EOS parameter, as delineated in Equation (24), in relation to the constrained values of parameters $w_0$ and $w_1$ determined from the CC+PPS+DESI BAO dataset. At $z = 0$, the EoS parameter's values are $\omega = -0.61$ (for $w_0 = -0.61, w_1 = 0.16$ the best fit values from the CC+PPS+DESI BAO dataset). Evolution of the effective EoS parameter $\Omega$ for the proposed $f(R, L_m)$ model and standard $\Lambda$CDM scenario, using the combined observational datasets (CC+PPS+DESI BAO). The $\Lambda$CDM curve exhibited the expected transition from a matter-dominated epoch $\omega = 0$ to the late-time acceleration phase $\omega = -1$.

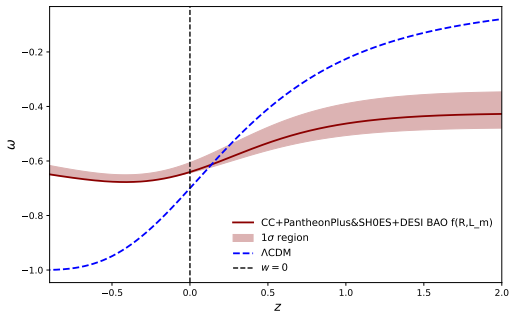


**Figure 5.** The graphical behavior of $\omega$ with $z$.

### *6.3. Energy Conditions*

In cosmology, energy conditions are formulations of the properties of the energy–momentum tensor $T_\mu\nu$ and correspond to various sets of inequalities that qualitatively distinguish between the normal stuff and the not-so-normal stuff comprising the universe. Such conditions are essential in general relativity and instrumental in investigating the evolution and structure of the universe. They are generally used to formulate general type theorems, using Hawking and Penrose's singular type theorems.

#### 6.3.1. Null Energy Condition (NEC)

The null energy condition is given by

$$\rho + p \geq 0 \tag{33}$$

In Figure 6, the absolute value of $\rho + p$ is strictly positive throughout the redshift $z$. This indicates that NEC is preserved throughout the entire span of the cosmic history given by this model. NEC satisfaction indicates that the model does not involve the presence of unphysical or exotic sources of matter, such as phantom energy, neither in the current epoch nor in the early universe. Moreover, following the NEC rules, the fast growth of the universe in this model is not caused by anything that breaks the normal cause-and-effect rules. Recent studies such as those in Refs. [63,97,98] also state that meeting NEC helps build dark energy models that work well with observations, including Planck data [3].

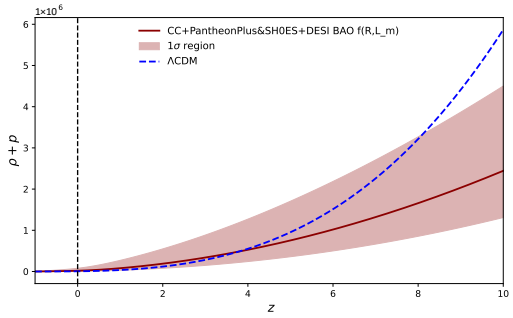


**Figure 6.** Graphical behavior of NEC versus redshift.

6.3.2. Dominant Energy Condition (DEC)

The dominant energy condition is given by

$$\rho - p \geq 0 \tag{34}$$

As shown in Figure 7, the DEC remains valid for all redshifts studied. The increase in $\rho - p$ as the redshift increases shows that in the early universe, the model suggests that the energy density was much stronger than the pressure. This makes sense because the early universe was mostly made of regular matter and energy, and the amount of energy was much greater than the amount of pressure. The fact that dark energy behaves in this way throughout the universe's history means that the model works properly and follows the usual rules of cause and effect.

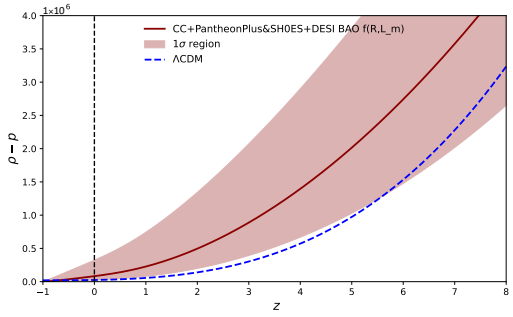


**Figure 7.** Graphical behavior of dominant energy condition versus redshift.

6.3.3. Strong Energy Condition (SEC)

The strong energy condition is given by

$$\rho + 3p \geq 0 \tag{35}$$

The active gravitational mass $(\rho + 3p)$ remains positive during the decelerated expansion phase. Nonetheless, there appears to have been some breach of this requirement between the galaxy formation era and the present, according to observational data. Therefore, if $\rho + 3p < 0$, the universe's accelerated expansion (or, equivalently, the beginning of repulsive gravity) might be observed. The possibility of negative cosmic pressure with anti gravitating effects is suggested by the inequality $\rho + 3p < 0$. Because the SEC involves two inequalities, it should be highlighted that a breach of either would be considered a violation of the SEC [99–101]. The Figure 8 illustrates that while the ΛCDM model preserves positive $\rho + 3p$ (no SEC violation), the $f(R, L_m)$ model yields negative $\rho + 3p$ values at late times, indicating accelerated expansion driven by the coupling between curvature and matter sectors.

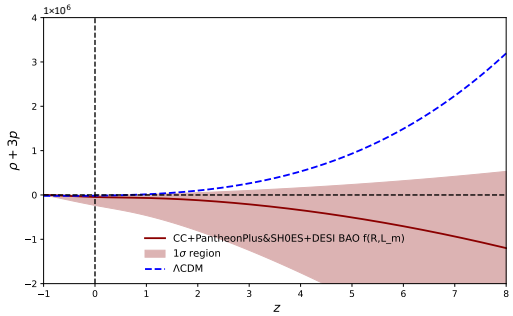


**Figure 8.** Graphical behavior of SEC versus redshift.

### *6.4. $Om(z)$ DIAGNOSTICS*

A geometric methodology was employed in cosmology, with the Hubble parameter serving as a crucial test for the ΛCDM model. The function $Om(z)$ probes the different dark energy theories and the ΛCDM model through the volume changes in its slope [102]. This is simple in that it depends only on the first-order derivative of the scaling factor. This makes it easy to use and understand in cosmological investigations. We can write a flat spatial universe as

$$Om(z) = \frac{\left(-\frac{H(z)}{H_0}\right)^2 + 1}{-(1+z)^3 + 1}, \tag{36}$$

where $H_0$ denotes the present value of the Hubble parameter. A quintessence or phantom nature can be indicated by a positive or negative slope of the $Om(z)$ diagnostic. A straight line in terms of the redshift from the test suggests the existence of a DE model, which is consistent with the cosmological concentration. Figure 9 shows that the $Om(z)$ diagnostic has a negative slope when considering the best values of the model parameters obtained by the combined (CC+PPS+DESI BAO) dataset. Overall, this deviation from the constant ΛCDM line highlights that the $f(R, L_m)$ model provides a richer cosmic evolution, capable of explaining late-time acceleration without invoking a pure cosmological constant, while is consistent with the observational data.

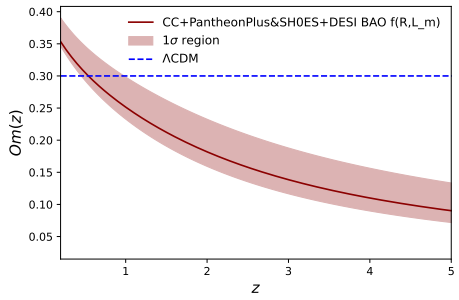


**Figure 9.** The graphical behavior of $Om(z)$ vs. $z$.

### *6.5. Age of the Universe*

The age of the universe can be estimated using the concept of lookback time, which represents the time interval between the present age of the universe $t_0$ and its age at a given redshift $z$ [31,103–105]. In a cosmological model where the Hubble parameter $H(z)$ varies with redshift, the lookback time is expressed through the following integral:

$$t_0 - t(z) = \int_0^z \frac{dz'}{(1+z')H(z')} \tag{37}$$

From Equations (26) and (37), we get

$$H_0(t_0 - t(z)) = \int_0^z \frac{dz'}{(1+z')(1+z)^{\frac{3n(1+\omega_0)}{2(2n-1)}}(1+z^2)^{\frac{3n\omega_1}{4(2n-1)}}} \tag{38}$$

The evolution of the lookback time as a function of redshift for both models is illustrated in Figure 10. For the parameter values $H_0 = 72.08^{+0.30}_{-0.24}$ km s$^{-1}$Mpc$^{-1}$, $n = 0.91^{+0.14}_{-0.21}$, $w_0 = 0.61 \pm 0.11$, $w_1 = 0.16^{+0.075}_{-0.092}$, using the posterior distributions of the cosmological parameters obtained from the MCMC analysis, we propagate the parameter uncertainties through Equation (37) to reconstruct the probability distribution of the present age of the universe. We obtain $t_0 = 15.62^{+0.85}_{-0.73}$ Gyr, where the quoted uncertainty reflects the combined contributions from $H_0$, $n$, $w_0$, and $w_1$.

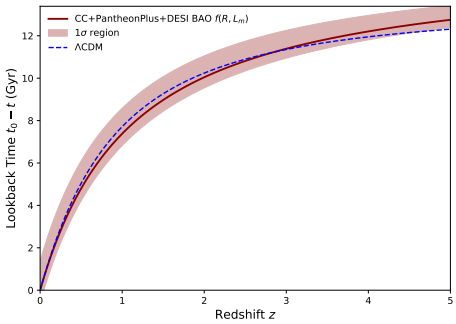


**Figure 10.** Comparison of lookback time as a function of redshift for the $f(R, L_m)$ model and the ΛCDM model.

**Statistical Analysis**: In the final step of the observational analysis, we compare the $f(R, L_m)$ and standard models through standard information criteria such as the Akaike Information Criterion (AIC) [106] and the Bayesian Information Criterion (BIC) [107]. Both of these are widely employed in statistics and data analysis and are described below.

$$\text{AIC} = -2\ln\mathcal{L} + 2k = \chi^2_{min} + 2k,$$

$$\text{BIC} = -2\ln\mathcal{L} + k\ln N = \chi^2_{min} + k\ln N,$$

In this expression, $\mathcal{L} = \exp(-\chi^2_{\text{min}}/2)$ yields the maximum likelihood, where $k$ is the number of free parameters in the model and $N$ is the total number of data points used in the experiment. Using the typical ΛCDM cosmology as a baseline scenario is crucial for assessing and contrasting other hypotheses. You can evaluate the relative performance of any model $M$ by computing the difference $\Delta X = X_M - X_{\Lambda\text{CDM}}$, where $X$ is the AIC or BIC. Based on the value of $\Delta X$, the model's level of support can be interpreted as follows: For the AIC, there is strong support if $\Delta\text{AIC} \leq 2$ (indicating a good fit), moderate support if $4 \leq \Delta\text{AIC} \leq 7$, and essentially no support if $\Delta\text{AIC} \geq 10$. For the BIC, the evidence is considered positive if $2 \leq \Delta\text{BIC} \leq 6$, strong if $6 < \Delta\text{BIC} \leq 10$, and *very strong* if $\Delta\text{BIC} > 10$.

The calculated values of AIC, BIC, and $\chi^2$ for our models are shown in Table 2, which compares them to the traditional ΛCDM cosmology using distinct observational datasets: CC, PPS, CC+PPS, and CC+PPS+DESI BAO. The relative differences between ΔAIC and ΔBIC in relation to the baseline ΛCDM model are also reported to enable a fair comparison. The AIC and BIC values of our model are marginally higher than those of the ΛCDM scenario across all of the datasets provided, which is significant. Because our model has more degrees of freedom, we obtain these larger values. Several papers are presented in the literature that have higher AIC and BIC values relative to the standard model [107–109], as cosmological models, despite sometimes yielding competitive or even superior fits, often

result in higher AIC and BIC values due to their enlarged parameter spaces. Hence, our results remain statistically consistent and in good agreement with the observational data.

**Table 2.** The difference, $\Delta\text{AIC} = \text{AIC}_{f(R,L_m)\,\text{Model}} - \text{AIC}_{\Lambda\text{CDM}}$ and $\Delta\text{BIC} = \text{BIC}_{f(R,L_m)\,\text{Model}} - \text{BIC}_{\Lambda\text{CDM}}$ for our model with respect to ΛCDM from all considered datasets.

| **Dataset** | **CC** | **PPS** | **CC+PPS** | **CC+PPS+DESI BAO** |
|---|---|---|---|---|
| **Model** | $f(R, L_m)$ **Model**<br>**ΛCDM** | $f(R, L_m)$ **Model**<br>**ΛCDM** | $f(R, L_m)$ **Model**<br>**ΛCDM** | $f(R, L_m)$ **Model**<br>**ΛCDM** |
| **AIC** | 41.56<br>38.08 | 1301.92<br>1298.14 | 1354.1<br>1351.64 | 1345.88<br>1342.08 |
| **Δ AIC** | 3.48 | 3.78 | 2.46 | 3.8 |
| **BIC** | 52.03<br>47.05 | 1339.99<br>1330.77 | 1392.30<br>1384.38 | 1384.13<br>1374.8 |
| **Δ BIC** | 4.98 | 9.22 | 7.92 | 9.33 |
| $\chi^2_{min}$ | 27.56<br>26.08 | 1287.92<br>1286.14 | 1340.1<br>1339.64 | 1331.88<br>1330.08 |

## 7. Conclusions

In this work, we have investigated the cosmological implications of the modified gravity framework $f(R, L_m)$ with the specific form $f(R, L_m) = \frac{R}{2} + L_m^n$, adopting the Barboza–Alcaniz parameterization of the dark energy equation of state. By deriving the Hubble parameter $H(z)$ within a flat FLRW background and constraining the parameters $(H_0, n, w_0, w_1)$ through a Bayesian MCMC analysis using CC, Pantheon, and PPS datasets, we obtained strong observational consistency of the model. Our analysis shows that the best-fit value of the Hubble constant from the CC+PPS+DESI BAO dataset, $H_0 = 72.08^{+0.30}_{-0.24}\,\text{km s}^{-1}\text{Mpc}^{-1}$, lies closer to the local SH0ES measurement than to the Planck CMB result. This indicates that the proposed $f(R, L_m)$ model significantly alleviates the well-known Hubble tension, reducing it from the $\sim 4.4\sigma$ discrepancy between Planck and SH0ES to approximately $\sim 1.4\sigma$. Moreover, the present values of the deceleration parameter ($q_0 < 0$) consistently confirm that the universe is undergoing an accelerated expansion.

The reconstructed equation of the state parameter, the evolution of the deceleration parameter, and the Om diagnostic further support the model's capability to describe late-time cosmic acceleration beyond the standard ΛCDM scenario. In particular, the negative slope of the Om diagnostic indicates phantom-like behavior of dark energy for the best-fit values of the parameters. Additionally, the estimated age of the universe in this framework, $t_0 \approx 15.62\,\text{Gyr}$, is in reasonable agreement with the current astrophysical observations. Overall, our findings demonstrate that $f(R, L_m)$ gravity with the chosen functional form provides a viable extension of general relativity, capable of explaining the late-time acceleration of the universe while simultaneously easing Hubble tension. Future work may explore broader parameterizations of the dark energy sector, nonlinear forms of $f(R, L_m)$, and the inclusion of other cosmological datasets such as BAO and CMB anisotropies, to further test the robustness of this modified gravity scenario.

**Author Contributions:** Conceptualization, A.P.; methodology, M.S.B.; software, S.V.; formal analysis, A.P.; investigation, A.D.; data curation, S.V.; writing—original draft preparation, S.V.; writing—review and editing, A.D. and A.P.; visualization, M.S.B.; project administration, A.D. All authors have read and agreed to the published version of the manuscript.

**Funding:** S. Verma is supported by a Senior Research Fellowship (UGC Ref No. 192180404148) from the University Grants Commission, New Delhi, India.

**Data Availability Statement:** We employed publicly available CMB data, Pantheon Plus SH0ES data, Cosmic Chronometer (CC) data, and DESI-DR1 data in this study. The CC data are compiled from publicly available cosmic chronometer measurements in the literature, with a representative compilation accessible at https://github.com/Ahmadmehrabi/Cosmic_chronometer_data (accessed on 25 February 2026).

**Acknowledgments:** The authors (A. Dixit and A. Pradhan) thank the Inter-University Centre for Astronomy and Astrophysics (IUCAA), Pune, India, for the support and resources offered under the visiting associateship program. The authors sincerely thank the reviewer and editor for their comments and suggestions, which improved the manuscript in its current form.

**Conflicts of Interest:** The authors declare no conflicts of interest.

## References

1. Riess, A.G.; Filippenko, A.V.; Challis, P.; Clocchiatti, A.; Diercks, A.; Garnavich, P.M.; Gilliland, R.L.; Hogan, C.J.; Jha, S.; Kirshner, R.P.; et al. Observational Evidence from Supernovae for an Accelerating Universe and a Cosmological Constant. *Astron. J.* **1998**, *116*, 1009–1038. [CrossRef]
2. Perlmutter, S.; Aldering, G.; Goldhaber, G.; Knop, R.A.; Nugent, P.; Castro, P.G.; Deustua, S.; Fabbro, S.; Goobar, A.; Groom, D.E.; et al. Measurements of Ω and Λ from 42 High-Redshift Supernovae. *Astrophys. J.* **1999**, *517*, 565–586. [CrossRef]
3. Aghanim, N.; Akrami, Y.; Ashdown, M.; Aumont, J.; Baccigalupi, C.; Ballardini, M.; Banday, A.; Barreiro, R.; Bartolo, N.; Basak, S.; et al. Planck 2018 results. VI. Cosmological parameters. *Astron. Astrophys.* **2020**, *641*, A6.
4. Weinberg, S. The cosmological constant problem. *Rev. Mod. Phys.* **1989**, *61*, 1. [CrossRef]
5. Ray, S.; Mukhopadhyay, U.; Meng, X.-H. Accelerating Universe with a dynamic cosmological term. *Grav. Cosmol.* **2007**, *13*, 142.
6. Usmani, A. The dark energy equation of state. *Mon. Not. R. Astron. Soc. Lett.* **2008**, *386*, L92–L95. [CrossRef]
7. Mukhopadhyay, U.; Ray, S.; Choudhury, S.B.D. Λ-CDM universe: A phenomenological approach with many possibilities. *Int. J. Mod. Phys. D* **2008**, *17*, 301–309. [CrossRef]
8. Ray, S.; Ray, P.C.; Khlopov, M.; Ghosh, P.P.; Mukhopadhyay, U.; Chowdhury, P. Scenario of inflationary cosmology from the phenomenological Λ models. *Int. J. Theor. Phys.* **2009**, *48*, 2499–2510. [CrossRef]
9. Mukhopadhyay, U.; Ray, P.C.; Ray, S.; Dutta Choudhury, S.B. Generalized Model for Λ Dark Energy. *Int. J. Mod. Phys. D* **2009**, *18*, 389–396. [CrossRef]
10. Singh, A.; Krishnannair, S. Varying vacuum models with spatial curvature: A dynamical system perspective. *Gen. Relativ. Grav.* **2024**, *56*, 31. [CrossRef]
11. Singh, A. Role of dynamical vacuum energy in the closed universe: Implications for bouncing scenario. *Gen. Relativ. Grav.* **2024**, *56*, 138. [CrossRef]
12. Caldwell, R.R.; Dave, R.; Steinhardt, P.J. Cosmological Imprint of an Energy Component with General Equation of State. *Phys. Rev. Lett.* **1998**, *80*, 1582–1585. [CrossRef]
13. Steinhardt, P.J.; Wang, L.; Zlatev, I. Cosmological tracking solutions. *Phys. Rev. D* **1999**, *59*, 123504. [CrossRef]
14. Kotambkar, S.; Singh, G.P.; Kelkar, R. Anisotropic cosmological models with quintessence. *Int. J. Theor. Phys.* **2014**, *53*, 449–460. [CrossRef]
15. Caldwell, R. A phantom menace? Cosmological consequences of a dark energy component with super-negative equation of state. *Phys. Lett. B* **2002**, *545*, 23–29. [CrossRef]
16. Elizalde, E.; Nojiri, S.; Odintsov, S.D. Late-time cosmology in a (phantom) scalar-tensor theory: Dark energy and the cosmic speed-up. *Phys. Rev. D* **2004**, *70*, 043539. [CrossRef]
17. Guo, Z.-K.; Piao, Y.-S.; Zhang, X.; Zhang, Y.-Z. Cosmological evolution of a quintom model of dark energy. *Phys. Lett. B* **2005**, *608*, 177–182. [CrossRef]
18. Zhao, W.; Zhang, Y. Quintom models with an equation of state crossing −1. *Phys. Rev. D* **2006**, *73*, 123509. [CrossRef]
19. Cai, Y.-F.; Saridakis, E.N.; Setare, M.R.; Xia, J.-Q. Quintom cosmology: Theoretical implications and observations. *Phys. Rep.* **2010**, *493*, 1–60. [CrossRef]
20. Patil, T.; Panda, S.; Sharma, M. Dynamics of interacting scalar field model in the realm of chiral cosmology. *Eur. Phys. J. C* **2023**, *83*, 131. [CrossRef]
21. Patil, T.; Panda, S. Coupled scalar field cosmology with effects of curvature. *Eur. Phys. J. Plus* **2023**, *138*, 1–11. [CrossRef]
22. Aich, A. Phenomenological dark energy model with hybrid dynamic cosmological constant. *Class. Quantum Grav.* **2022**, *39*, 035010. [CrossRef]
23. Copeland, E.J.; Sami, M.; Tsujikawa, S. Dynamics of dark energy. *Int. J. Mod. Phys. D* **2006**, *15*, 1753–1935. [CrossRef]

24. Di Valentino, E.; Said, J.L.; Riess, A.; Pollo, A.; Poulin, V.; Gómez-Valent, A.; Weltman, A.; Palmese, A.; Huang, C.D.; van de Bruck, C.; et al. The CosmoVerse White Paper: Addressing observational tensions in cosmology with systematics and fundamental physics. *Phys. Dark Universe* **2025**, *49*, 101965. [CrossRef]
25. Hernandez, M.L.; De-Santiago, J. Is there a dynamical tendency in $H_0$ with late time measurements? *J. Cosmol. Astropart. Phys.* **2025**, *3*, 026. [CrossRef]
26. Jia, X.D.; Hu, J.P.; Gao, D.H.; Yi, S.X.; Wang, F.Y. The Hubble Tension Resolved by the DESI Baryon Acoustic Oscillations Measurements. *Astrophys. J.* **2025**, *994*, L22. [CrossRef]
27. Banik, I.; Samaras, N. Constraints on the Hubble and matter density parameters with and without modelling the CMB anisotropies. *Astronomy* **2025**, *4*, 24. [CrossRef]
28. Perivolaropoulos, L. Hubble tension or distance ladder crisis? *Phys. Rev. D* **2024**, *110*, 123518. [CrossRef]
29. Domínguez, A.; Kirkeberg, P.Ø.; Wojtak, R.; Saldana-Lopez, A.; Desai, A.; Primack, J.R.; Finke, J.; Ajello, M.; Pérez-González, P.G.; Paliya, V.S.; et al. A new derivation of the Hubble constant from $\gamma$-ray attenuation using improved optical depths for the Fermi and CTA era. *Mon. Not. R. Astron. Soc.* **2024**, *527*, 4632. [CrossRef]
30. Banik, I.; Kalaitzidis, V. Testing the local void hypothesis using baryon acoustic oscillation measurements over the last 20 yr. *Mon. Not. R. Astron. Soc.* **2025**, *540*, 545. [CrossRef]
31. Haslbauer, M.; Banik, I.; Kroupa, P. The KBC void and Hubble tension contradict ΛCDM on a Gpc scale —Milgromian dynamics as a possible solution. *Mon. Not. R. Astron. Soc.* **2020**, *499*, 2845. [CrossRef]
32. Kerner, R. Cosmology without singularity and nonlinear gravitational Lagrangians. *Gen. Relativ. Gravit.* **1982**, *14*, 453–469. [CrossRef]
33. Buchdahl, H.A. Non-linear Lagrangians and cosmological theory. *Mon. Not. R. Astron. Soc.* **1970**, *150*, 1–8. [CrossRef]
34. Carroll, S.M.; Duvvuri, V.; Trodden, M.; Turner, M.S. Is cosmic speed-up due to new gravitational physics? *Phys. Rev. D* **2004**, *70*, 043528. [CrossRef]
35. Capozziello, S.; Nojiri, S.; Odintsov, S.; Troisi, A. Cosmological viability of $f(R)$ gravity as an ideal fluid and its compatibility with a matter-dominated phase. *Phys. Lett. B* **2006**, *639*, 135–143. [CrossRef]
36. Amendola, L.; Polarski, D.; Tsujikawa, S. Are f(R) dark energy models cosmologically viable? *Phys. Rev. Lett.* **2007**, *98*, 131302. [CrossRef]
37. Nojiri, S.; Odintsov, S.D. Modified gravity with negative and positive powers of curvature: Unification of inflation and cosmic acceleration. *Phys. Rev. D* **2003**, *68*, 123512. [CrossRef]
38. Faraoni, V. Solar system experiments do not yet veto modified gravity models. *Phys. Rev. D* **2006**, *74*, 023529. [CrossRef]
39. Zhang, P. Behavior of f(R) gravity in the solar system, galaxies, and clusters. *Phys. Rev. D* **2007**, *76*, 024007. [CrossRef]
40. Amendola, L.; Tsujikawa, S. Phantom crossing, equation-of-state singularities, and local gravity constraints in f(R) models. *Phys. Lett. B* **2008**, *660*, 125–132. [CrossRef]
41. Starobinsky, A.A. Disappearing cosmological constant in f(R) gravity. *JETP Lett.* **2007**, *86*, 157–163. [CrossRef]
42. Tsujikawa, S. Observational signatures of f(R) dark energy models that satisfy cosmological and local gravity constraints. *Phys. Rev. D* **2008**, *77*, 023507. [CrossRef]
43. Capozziello, S.; Tsujikawa, S. Solar system and equivalence principle constraints on f(R) gravity by the chameleon approach. *Phys. Rev. D* **2008**, *77*, 107501. [CrossRef]
44. Liu, T.; Zhang, X.; Zhao, W. Constraining f(R) gravity in solar system, cosmology and binary pulsar systems. *Phys. Lett. B* **2018**, *777*, 286–293. [CrossRef]
45. Nojiri, S.; Odintsov, S.D. Gravity assisted dark energy dominance and cosmic acceleration. *Phys. Lett. B* **2004**, *599*, 137–142. [CrossRef]
46. Allemandi, G.; Borowiec, A.; Francaviglia, M.; Odintsov, S.D. Dark energy dominance and cosmic acceleration in first-order formalism. *Phys. Rev. D* **2005**, *72*, 063505. [CrossRef]
47. Nojiri, S.; Odintsov, S.D. Modified f(R) gravity consistent with realistic cosmology: From a matter-dominated epoch to a dark energy universe. *Phys. Rev. D* **2006**, *74*, 086005. [CrossRef]
48. Nojiri, S.; Odintsov, S.D. Newton law corrections and instabilities in f(R) gravity with the effective cosmological constant epoch. *Phys. Lett. B* **2007**, *652*, 343–348. [CrossRef]
49. Nojiri, S.; Odintsov, S.D. Unifying inflation with ΛCDM epoch in modified f(R) gravity consistent with Solar System tests. *Phys. Lett. B* **2007**, *657*, 238–245. [CrossRef]
50. Cognola, G.; Elizalde, E.; Nojiri, S.; Odintsov, S.D.; Sebastiani, L.; Zerbini, S. Class of viable modified f(R) gravities describing inflation and the onset of accelerated expansion. *Phys. Rev. D* **2008**, *77*, 046009. [CrossRef]
51. Nojiri, S.; Odintsov, S.D. Modified f(R) gravity unifying $R^m$ inflation with the ΛCDM epoch. *Phys. Rev. D* **2008**, *77*, 026007. [CrossRef]
52. Bertolami, O.; Böhmer, C.G.; Harko, T.; Lobo, F.S.N. Extra force in f(R) modified theories of gravity. *Phys. Rev. D* **2007**, *75*, 104016. [CrossRef]

53. Faraoni, V. Viability criterion for modified gravity with an extra force. *Phys. Rev. D* **2007**, *76*, 127501. [CrossRef]
54. Santos, J.; Alcaniz, J.S.; Reboucas, M.J.; Carvalho, F.C. Energy conditions in f(R) gravity. *Phys. Rev. D* **2007**, *76*, 083513. [CrossRef]
55. Bamba, K.; Geng, C.-Q.; Nojiri, S.; Odintsov, S.D. Crossing of the phantom divide in modified gravity. *Phys. Rev. D* **2009**, *79*, 083014. [CrossRef]
56. Harko, T. Modified gravity with arbitrary coupling between matter and geometry. *Phys. Lett. B* **2008**, *669*, 376–379. [CrossRef]
57. Capozziello, S.; Cardone, V.F.; Salzano, V. Cosmography of f(R) gravity. *Phys. Rev. D* **2008**, *78*, 063504. [CrossRef]
58. Nojiri, S.; Odintsov, S.D.; Sáez-Gómez, D. Cosmological reconstruction of realistic modified F(R) gravities. *Phys. Lett. B* **2009**, *681*, 74–80. [CrossRef]
59. Faraoni, V. Lagrangian description of perfect fluids and modified gravity with an extra force. *Phys. Rev. D* **2009**, *80*, 124040. [CrossRef]
60. Nojiri, S.; Odintsov, S.D. Unified cosmic history in modified gravity: From F(R) theory to Lorentz non-invariant models. *Phys. Rep.* **2011**, *505*, 59–144. [CrossRef]
61. Elizalde, E.; Myrzakulov, R.; Obukhov, V.V.; Sáez-Gómez, D. Nonsingular exponential gravity: A simple theory for early-and late-time accelerated expansion. *Phys. Rev. D* **2011**, *83*, 086006. [CrossRef]
62. Odintsov, S.D.; Gómez, D.S.-C.; Sharov, G.S. Is exponential gravity a viable description for the whole cosmological history? *Eur. Phys. J. C* **2017**, *77*, 862. [CrossRef]
63. Nojiri, S.; Odintsov, S.; Oikonomou, V. Modified gravity theories on a nutshell: Inflation, bounce and late-time evolution. *Phys. Rep.* **2017**, *692*, 1–104. [CrossRef]
64. Nunes, R.C.; Pan, S.; Saridakis, E.N.; Abreu, E.M. New observational constraints on f(R) gravity from cosmic chronometers. *J. Cosmol. Astropart. Phys.* **2017**, *2017*, 005. [CrossRef]
65. Singh, G.P.; Hulke, N.; Singh, A. Cosmological study of particle creation in higher derivative theory. *Indian J. Phys.* **2020**, *94*, 127–141. [CrossRef]
66. Mishra, B.; Agrawal, A.S.; Tripathy, S.K.; Ray, S. Wormhole solutions in f(R) gravity. *Int. J. Mod. Phys. D* **2021**, *30*, 2150061. [CrossRef]
67. de Haro, J.; Amorós, J.; Odintsov, S.D. Finite-time cosmological singularities and the possible fate of the Universe. *Phys. Rep.* **2023**, *1034*, 1–114. [CrossRef]
68. Odintsov, S.D.; Oikonomou, V.; Sharov, G.S. Early dark energy with power-law F(R) gravity. *Phys. Lett. B* **2023**, *843*, 137988. [CrossRef]
69. Nesseris, S. Matter density perturbations in modified gravity models with arbitrary coupling between matter and geometry. *Phys. Rev. D* **2009**, *79*, 044015. [CrossRef]
70. Harko, T. Galactic rotation curves in modified gravity with nonminimal coupling between matter and geometry. *Phys. Rev. D* **2010**, *81*, 084050. [CrossRef]
71. Harko, T. The matter Lagrangian and the energy-momentum tensor in modified gravity with nonminimal coupling between matter and geometry. *Phys. Rev. D* **2010**, *81*, 044021. [CrossRef]
72. Harko, T.; Lobo, F.S.N. $f(R, L_m)$ gravity. *Eur. Phys. J. C* **2010**, *70*, 373–379. [CrossRef]
73. Faraoni, V. *Cosmology in Scalar Tensor Gravity*; Springer: Durham, NC, USA, 2004.
74. Rahaman, F.; Ray, S.; Kalam, M.; Sarker, M. Do solar system tests permit higher dimensional general relativity? *Int. J. Theor. Phys.* **2009**, *48*, 3124. [CrossRef]
75. Matos, I.S.; Calvão, M.O.; Waga, I. Gravitational wave propagation in f(r) models: New parametrizations and observational constraints. *Phys. Rev. D* **2021**, *103*, 104059. [CrossRef]
76. Lobo, F.S.N.; Harko, T. Extended $f(R, L_m)$ theories of gravity. In *Proceedings of the Thirteenth Marcel Grossmann Meeting on Recent Developments in Theoretical and Experimental General Relativity, Astrophysics and Relativistic Field Theories*; World Scientific: Singapore, 2015.
77. Shukla, A.; Raushan, R.; Chaubey, R. Dynamical systems analysis of $f(R, L_m)$ gravity model. *Int. J. Geom. Methods Mod. Phys.* **2025**, *22*, 2550118. [CrossRef]
78. Ryden, B. *Introduction to Cosmology*; Addison Wesley: San Francisco, CA, USA, 2003.
79. Harko, T.; Lobo, F.S. Generalized curvature–matter couplings in modified gravity. *Galaxies* **2014**, *2*, 410–465. [CrossRef]
80. Harko, T.; Lobo, F.S.N.; Mimoso, J.P.; Pavón, D. Gravitational induced particle production through a nonminimal curvature–matter coupling. *Eur. Phys. J. C* **2015**, *75*, 386. [CrossRef]
81. Jassal, H.K.; Bagla, J.S.; Padmanabhan, T. Observational constraints on low redshift evolution of dark energy: How consistent are dierent observations. *Phys. Rev. D* **2005**, *72*, 103503. [CrossRef]
82. Brout, D.; Scolnic, D.; Popovic, B.; Riess, A.G.; Carr, A.; Zuntz, J.; Kessler, R.; Davis, T.M.; Hinton, S.; Jones, D.; et al. The Pantheon+ Analysis: Cosmological Constraints. *Astrophys. J.* **2022**, *938*, 110. [CrossRef]
83. Jimenez, R.; Loeb, A. Constraining cosmological parameters based on relative galaxy ages. *Astrophys. J.* **2002**, *573*, 37. [CrossRef]

84. Moresco, M.; Pozzetti, L.; Cimatti, A.; Jimenez, R.; Maraston, C.; Verde, L.; Thomas, D.; Citro, A.; Tojeiro, R.; Wilkinson, D. A 6% measurement of the Hubble parameter at $z \sim 0.45$ : Direct evidence of the epoch of cosmic re-acceleration. *J. Cosmol. Astropart. Phys.* **2016**, *2016*, 014. [CrossRef]
85. Moresco, M. Raising the bar: New constraints on the Hubble parameter with cosmic chronometers at $z \sim 2$. *Mon. Not. R. Astron. Soc. Lett.* **2015**, *450*, L16. [CrossRef]
86. Simon, J.; Verde, L.; Jimenez, R. Constraints on the redshift dependence of the dark energy potential. *Phys. Rev. D* **2005**, *71*, 123001. [CrossRef]
87. Stern, D.; Jimenez, R.; Verde, L.; Kamionkowski, M.; Stanford, S.A. Cosmic chronometers: Constraining the equation of state of dark energy. I: H(z) measurements. *J. Cosmol. Astropart. Phys.* **2010**, *2010*, 008.
88. Zhang, C.; Zhang, H.; Yuan, S.; Liu, S.; Zhang, T.-J.; Sun, Y.-C. Four new observational H(z) data from luminous red galaxies in the Sloan Digital Sky Survey data release seven. *Res. Astron. Astrophys.* **2014**, *14*, 1221. [CrossRef]
89. Riess, A.G.; Macri, L.M.; Hoffmann, S.L.; Scolnic, D.; Casertano, S.; Filippenko, A.V.; Tucker, B.E.; Reid, M.J.; Jones, D.O.; Silverman, J.M.; et al. A 2.4% determination of the local value of the Hubble constant. *Astrophys. J.* **2016**, *826*, 56. [CrossRef]
90. Jiao, K.; Zhang, T.J.; Gao, L. FLRW Kinematic-Induced Measurement of the Hubble Constant from Cosmic Chronometer and Redshift Drift Observations. *arXiv* **2025**, arXiv:2506.16669v2. [CrossRef]
91. Adame, A.; Aguilar, J.; Ahlen, S.; Alam, S.; Alexander, D.; Alvarez, M.; Alves, O.; Anand, A.; Andrade, U.; Armengaud, E.; et al. DESI 2024 VI: Cosmological constraints from the measurements of baryon acoustic oscillations. *J. Cosmol. Astropart. Phys.* **2025**, *2*, 021. [CrossRef]
92. Odintsov, S.D.; Gómez, D.S.-C.; Sharov, G.S. Modified gravity/dynamical dark energy vs ΛCDM: Is the game over? *Eur. Phys. J. C* **2025**, *85*, 298. [CrossRef]
93. Foreman-Mackey, D.; Hogg, D.W.; Lang, D.; Goodman, J. emcee: The MCMC hammer. *Publ. Astron. Soc. Pac.* **2013**, *125*, 306. [CrossRef]
94. Jaybhaye, L.V.; Solanki, R.; Mandal, S.; Sahoo, P.K. Cosmology in $f(R, L_m)$ gravity. *Phys. Lett. B* **2022**, *831*, 137148. [CrossRef]
95. Chaudhary, H.; Molla, N.U.; Khurana, M.; Debnath, U.; Mustafa, G. Cosmological test of dark energy parametrizations in Horava-Lifshitz gravity. *Eur. Phys. J. C* **2024**, *84*, 223. [CrossRef]
96. Yadav, A.K.; Bhoyar, S.; Dhabe, M.; Shekh, S.; Ahmad, N. Reconstructing $f(q)$ gravity from parameterization of the Hubble parameter and observational constraints. *J. High Energy Astrophys.* **2024**, *43*, 114–125. [CrossRef]
97. Bamba, K.; Capozziello, S.; Nojiri, S.; Odintsov, S.D. Dark energy cosmology: The equivalent description via different theoretical models and cosmography tests. *Astrophys. Space Sci.* **2012**, *342*, 155. [CrossRef]
98. Wang, J.; Liao, K. Energy conditions in $f(R, L_m)$ gravity. *Class. Quantum Gravity* **2012**, *29*, 215016. [CrossRef]
99. Singh, A.; Raushan, R.; Chaubey, R.; Mandal, S.; Mishra, K.C. Lagrangian formulation and implications of barotropic fluid cosmologies. *Int. J. Geom. Methods Mod. Phys.* **2022**, *19*, 2250107. [CrossRef]
100. Singh, A. Homogeneous and anisotropic cosmologies with affine EoS: A dynamical system perspective. *Eur. Phys. J. C* **2023**, *83*, 696. [CrossRef]
101. Lalke, A.R.; Singh, G.P.; Singh, A. Late-time acceleration from ekpyrotic bounce in $f(q, t)$ gravity. *Int. J. Geom. Methods Mod. Phys.* **2023**, *20*, 2350131. [CrossRef]
102. Sahni, V.; Shafieloo, A.; Starobinsky, A.A. Two new diagnostics of dark energy. *Phys. Rev. D* **2008**, *78*, 103502. [CrossRef]
103. Valcin, D.; Jimenez, R.; Seljak, U.; Verde, L. The Age of the Universe with Globular Clusters III: Gaia distances and hierarchical modeling. *arXiv* **2025**, arXiv:2503.19481. [CrossRef]
104. Xiang, M.; Rix, H.W.A. time-resolved picture of our Milky Way's early formation history. *Nature* **2022**, *603*, 599–603. [CrossRef] [PubMed]
105. Xiang, M.; Rix, H.-W.; Yang, H.; Liu, J.; Huang, Y.; Frankel, N. The formation and survival of the Milky Way's oldest stellar disk. *Nat. Astron.* **2025**, *9*, 101–110. [CrossRef]
106. Schwarz, G.E. Estimating the dimension of a model. *Ann. Statist.* **1978**, *6*, 461. [CrossRef]
107. Xu, Y.-Y.; Zhang, X. Comparison of dark energy models after Planck 2015. *Eur. Phys. J. C* **2016**, *76*, 588. [CrossRef]
108. Rezaei, M.; Malekjani, M. Comparison between different methods of model selection in cosmology. *Eur. Phys. J. Plus* **2021**, *136*, 219. [CrossRef]
109. Zhu, X.; Xu, R.; Xu, D. Bumblebee cosmology: Tests using distance-and time-redshift probes. *arXiv* **2024**, arXiv:2411.18559. [CrossRef]